Canadian Science Publishing
NRC Research Press journals | Publishing Services

Canadian Journal of Physics
Revue canadienne de physique

Physical Behavior of Anisotropic Compact Stars in f(R,T,RμνTμν) Gravity

Journal:	*Canadian Journal of Physics*
Manuscript ID	cjp-2016-0385.R1
Manuscript Type:	Article
Date Submitted by the Author:	26-Jul-2016
Complete List of Authors:	Sharif, M.; University of the Punjab, Waseem, Arfa; University of the Punjab
Keyword:	Compact Stars, Modified gravity, Anisotropic Fluid, Energy conditions, Stability

Physical Behavior of Anisotropic Compact Stars in $f(R,T,R_{\mu\nu}T^{\mu\nu})$ Gravity

M. Sharif *and Arfa Waseem †
Department of Mathematics, University of the Punjab,
Quaid-e-Azam Campus, Lahore-54590, Pakistan.

Abstract

This paper investigates the behavior of anisotropic compact stars in the background of $R+\alpha R_{\mu\nu}T^{\mu\nu}$ gravity model. For this purpose, we use Krori-Barua metric solutions where constants are calculated using masses and radii of compact stars like Her X-1, SAX J 1808.4-3658 and 4U1820-30. We analyze regular behavior of effective energy density, radial and transverse pressures in the interior of compact stars. We also discuss energy conditions, effect of anisotropic factor and stability criteria of these stars. It is concluded that the considered compact star models satisfy all the energy conditions and remain stable against the anisotropic effect in this gravity.

Keywords: Compact Stars; $f(R,T,R_{\mu\nu}T^{\mu\nu})$ gravity.
PACS: 04.50.Kd; 97.60.Jd.

1 Introduction

Observational facts and theoretical predictions explore many hidden constituents of the universe and deduce that a huge part of this mysterious

*msharif.math@pu.edu.pk
†arfawaseem6@hotmail.com

universe comprises stars, clusters and galaxies. The study of these relativistic objects motivates researchers to investigate their physical behavior and different evolutionary stages in cosmology and astrophysics. The strong gravitational pull disturbs the stable structure of a star and consequently, the star emits visible light in our universe. Stars are formed from the gaseous clouds of hydrogen and its evolution starts due to nuclear reactions occurring in the core of a star. This nuclear reaction converts the hydrogen cloud into helium which releases a large amount of electromagnetic radiations. In the interior of a star, if the nuclear fuel is exhausted completely and the gravitational force dominates the thermal pressure, then star collapses which leads to the formation of stellar remnants known as compact stars. Recently, a large number of compact stars are discovered in the universe which possess very strong magnetic fields and high densities. The revolutionary formation of these stars leads to neutron stars, black holes and white dwarfs depending on their masses.

After the discovery of neutron, Baade and Zwicky [1] introduced the concept of neutron stars whose interesting properties and structure captivated the attention of many researchers. Due to different pulse periods, the neutron stars incorporate X-ray pulsar Her X-1, Millisecond pulsar SAX J 1808.4-3658 and X-ray burster 4U 1820-30. The isotropic as well as anisotropic fluid distribution play a fundamental role to understand the interior structure and evolutionary stages of compact stars. An interesting discussion about anisotropic internal distribution of compact stars is given in [2]. In the interior of anisotropic compact stars, it is found that pressure is distributed into radial and transverse components. Hossein et al. [3] studied the behavior of compact stars with cosmological constant using anisotropic matter distribution in the interior region. Lobo [4] investigated the effect of anisotropic pressure in these stars via barotropic equation of state (EoS).

In order to investigate physical behavior and stability criteria of compact stars, numerical as well as analytical approaches have been used. Hernandez and Nunez [5] discussed static spherically symmetric anisotropic solutions of neutron stars and also analyzed equilibrium structure of stars via anisotropic Tolman-Oppenheimer-Volkoff (TOV) equation. Mak and Harko [6] obtained exact solution of the Einstein field equations for static spherically symmetric anisotropic matter distribution and investigated physical characteristics as well as stability of compact stars. For the same spacetime, a new class of relativistic solutions was established for anisotropic compact objects which preserve hydrostatic equilibrium [7]. The energy conditions, TOV equation

and stability condition of rotating neutron stars are also discussed for different scenarios [8].

Cosmological observations like cosmic microwave background, Wilkinson microwave anisotropy probe and large scale structure surveys [9] observed that the current universe comprises some mysterious form of energy and matter known as dark energy and dark matter, respectively. To investigate these mysterious constituents of the universe, modified theories of gravity are referred as the most excited approaches. These theories are classified into $f(R)$ (R represents Ricci scalar), $f(\mathcal{T})$ ($\mathcal{T}$ denotes torsion), $f(G)$ (G shows Gauss-Bonnet invariant term), $f(R,T)$ (T indicates the trace of energy-momentum tensor) [10] and $f(R,T,R_{\mu\nu}T^{\mu\nu})$ gravity [11].

The study of compact stars established very interesting results in general relativity as well as modified theories of gravity. Mak and Harko [12] analyzed anisotropic and isotropic configurations of compact stars for Einstein-Hilbert action. They discussed the effect of energy density, pressure and speed of sound while mass-radius relation is also obtained for stable structure of compact stars. Goswami et al. [13] found analytic solutions of a collapsing star with anisotropic pressure and heat flux in $f(R)$ gravity. The stability of neutron stars is also studied in $f(R)$ gravity [14]. Zubair et al. [15] analyzed the stability and formation of anisotropic compact stars in $f(R,T)$ gravity. Abbas et al. [16] examined physical properties as well as equilibrium condition of compact stars in $f(G)$ gravity. They found regular behavior of energy density, pressure and speed of sound in the interior of compact stars. The evolutionary stage, physical behavior and numerical solutions of compact stars are also studied in $f(\mathcal{T})$ gravity [17].

Due to non-minimal coupling of matter and geometry, the $f(R,T,R_{\mu\nu}T^{\mu\nu})$ gravity being the more generalized form of $f(R,T)$ gravity has gained much attention. Odinstov and Sáez-Gómes [18] investigated ΛCDM model, de Sitter solutions and matter instability in this theory. Haghani et al. [11] formulated the field equations corresponding to conservative and non-conservative physical systems while laws of thermodynamics [19] and energy conditions [20] are also discussed in this gravity.

In this paper, we explore anisotropic configuration of compact stars in this theory. The paper is organized as follows. In section **2**, we formulate the corresponding field equations for two different choices of matter Lagrangian. The physical features and stability of considered compact stars are given in section **3**. In the last section, we conclude our results.

2 Field Equations of $f(R,T,R_{\mu\nu}T^{\mu\nu})$ Gravity

The action of $f(R,T,R_{\mu\nu}T^{\mu\nu})$ gravity is defined as [11]

$$I=\frac{1}{2\kappa^2}\int d^4x\sqrt{-g}[f(R,T,R_{\mu\nu}T^{\mu\nu})+\mathcal{L}_m], \tag{1}$$

with gravitational coupling constant $\kappa^2=8\pi G=1$. The energy-momentum tensor is

$$T^{\mu\nu}=\frac{2}{\sqrt{-g}}\frac{\delta(\sqrt{-g}\mathcal{L}_m)}{\delta g_{\mu\nu}}=g^{\mu\nu}\mathcal{L}_m+\frac{2\delta\mathcal{L}_m}{\delta g_{\mu\nu}}. \tag{2}$$

By varying the action (1) with respect to $g^{\mu\nu}$, we obtain the field equations

$$G_{\mu\nu}=R_{\mu\nu}-\frac{1}{2}Rg_{\mu\nu}=T^{eff}_{\mu\nu}, \tag{3}$$

where the effective energy-momentum tensor is

$$\begin{aligned}T^{eff}_{\mu\nu} &= \frac{1}{f_R-f_Q\mathcal{L}_m}[(1+f_T+\frac{1}{2}Rf_Q)T_{\mu\nu}+\{\frac{1}{2}(f-Rf_R)-\mathcal{L}_m f_T\\ &- \frac{1}{2}\nabla_\alpha\nabla_\beta(f_QT^{\alpha\beta})\}g_{\mu\nu}-(g_{\mu\nu}\Box-\nabla_\mu\nabla_\nu)f_R+\nabla_\alpha\nabla_{(\mu}[T^\alpha_{\nu)}f_Q]\\ &- \frac{1}{2}\Box(f_QT_{\mu\nu})-2f_QR_{\alpha(\mu}T^\alpha_{\nu)}+2(f_Tg^{\alpha\beta}+f_QR^{\alpha\beta})\frac{\partial^2\mathcal{L}_m}{\partial g^{\mu\nu}\partial g^{\alpha\beta}}].\end{aligned} \tag{4}$$

Here $Q=R_{\mu\nu}T^{\mu\nu}$ and subscripts of generic function f represent derivative with respect to R, Q and T.

To describe the interior region of compact stars, the line element of static spherically symmetric metric is

$$ds^2_-=e^{\mu(r)}dt^2-e^{\nu(r)}dr^2-r^2(d\theta^2+\sin^2\theta d\phi^2), \tag{5}$$

where r represents radius of the star while $\mu(r)=Br^2+C$ and $\nu(r)=Ar^2$ are solutions of Krori-Barua metric which provide the rational modeling of compact stars [21]. The arbitrary constants A, B and C can be evaluated through some matching conditions [22]. We take the energy-momentum tensor in the form

$$T^{(matter)}_{\mu\nu}=(\rho+p_t)u_\mu u_\nu-p_tg_{\mu\nu}+(p_r-p_t)v_\mu v_\nu, \tag{6}$$

where $u_\mu = e^{\frac{\mu}{2}}\delta^0_\mu$ and $v_\mu = e^{\frac{\nu}{2}}\delta^1_\mu$ denote four velocity and radial four-vector, respectively whereas ρ, p_r and p_t represent energy density, radial and transverse pressures, respectively. To discuss the effect of non-minimal coupling between geometry and matter parts in the interior of compact stars, we consider a particular model of $f(R,T,R_{\mu\nu}T^{\mu\nu})$ gravity given by [11]

$$f(R,T,R_{\mu\nu}T^{\mu\nu}) = R + \alpha R_{\mu\nu}T^{\mu\nu}, \tag{7}$$

where α is a coupling constant. This model includes strong coupling of the Ricci and energy-momentum tensors. For this model, the field equations take the following form

$$\begin{aligned}
\rho^{eff} &= \frac{1}{1-\alpha\mathcal{L}_m}[\rho + \alpha\rho e^{-\nu}(\frac{15}{16}\mu'^2 + \frac{7}{8}\mu'' - \frac{\nu'}{r} - \frac{7}{16}\mu'\nu' + \frac{1}{r^2} + \frac{7}{4}\frac{\mu'}{r} - \frac{1}{r^2}e^{\nu}) \\
&+ \alpha\rho' e^{-\nu}(\frac{9}{8}\mu' - \frac{\nu'}{4} + \frac{1}{r}) + \alpha p_r e^{-\nu}(\frac{3}{16}\mu'\nu' - \frac{\mu''}{8} + \frac{3\nu'}{4r} - \frac{1}{2r^2} - \frac{1}{16}\mu'^2) \\
&+ \frac{\alpha}{4}(2\rho'' - p_r'')e^{-\nu} + \alpha p_r' e^{-\nu}(\frac{\nu'}{8} - \frac{\mu'}{4} - \frac{3}{4r}) + \alpha p_t e^{-\nu}(\frac{\mu'}{4r} + \frac{\nu'}{4r} + \frac{1}{2r^2}) \\
&+ \frac{\alpha}{2r}p_t' e^{-\nu}],
\end{aligned} \tag{8}$$

$$\begin{aligned}
p_r^{eff} &= \frac{1}{1-\alpha\mathcal{L}_m}[p_r + \alpha p_r e^{-\nu}(\frac{5}{16}\mu'^2 + \frac{3}{4}\nu'^2 + \frac{5}{8}\mu'' + \nu'' - \frac{3\nu'}{4r} - \frac{7}{16}\mu'\nu' + \frac{3}{2r^2} \\
&+ \frac{\mu'}{r} - \frac{1}{r^2}e^{\nu}) + \alpha p_r' e^{-\nu}(\frac{\mu'}{2} + \frac{5}{8}\nu' + \frac{7}{4r}) + \frac{3\alpha}{4}p_r'' e^{-\nu} + \alpha\rho e^{-\nu}(\frac{\mu'^2}{16} - \frac{1}{16}\mu' \\
&\times \nu' + \frac{\mu'}{4r} + \frac{\mu''}{8}) - \alpha p_t e^{-\nu}(\frac{\mu'}{4r} + \frac{\nu'}{4r} + \frac{1}{2r^2}) + \frac{\alpha}{8}\mu'\rho' e^{-\nu} + \frac{\alpha}{2r}p_t' e^{-\nu}],
\end{aligned} \tag{9}$$

$$\begin{aligned}
p_t^{eff} &= \frac{1}{1-\alpha\mathcal{L}_m}[p_t + \alpha p_t e^{-\nu}(\frac{\mu'^2}{4} + \frac{\mu''}{2} + \frac{\nu'}{4r} - \frac{1}{4}\mu'\nu' + \frac{11}{2r^2} + \frac{5\mu'}{4r} - \frac{1}{r^2}e^{\nu}) + \alpha \\
&\times p_t' e^{-\nu}(\frac{\mu'}{4} - \frac{\nu'}{4} + \frac{7}{2r}) + \frac{\alpha}{4}(2p_t'' + p_r'')e^{-\nu} + \alpha\rho e^{-\nu}(\frac{\mu'^2}{16} + \frac{\mu''}{8} + \frac{\mu'}{4r} - \frac{1}{16}\mu' \\
&\times \nu') + \alpha p_r e^{-\nu}(\frac{\mu'^2}{16} + \frac{\mu''}{8} - \frac{3}{16}\mu'\nu' - \frac{3\nu'}{4r} + \frac{1}{r^2}) + \frac{\alpha}{8}\mu'\rho' e^{-\nu} + \alpha p_r' e^{-\nu} \\
&\times (\frac{\mu'}{4} - \frac{\nu'}{8} + \frac{3}{4r})].
\end{aligned} \tag{10}$$

In order to simplify the field equations, we take $\rho = \frac{m}{V}$, where m denotes masses of the considered compact stars and $V = \frac{4}{3}\pi r^3$. We consider two different choices for matter Lagrangian, i.e., $\mathcal{L}_m = -p_r$ and $\mathcal{L}_m = -p_t$, where $p_t = (1+\beta)p_r$, $p_r = \frac{1}{3}\rho$ and $\beta > 0$ [23]. By applying Krori-Barua

metric solutions and substituting the values of ρ, p_r and p_t in Eqs.(8)-(10), the field equations for $\mathcal{L}_m = -p_r$ turn out to be

$$\begin{aligned}
\rho^{eff} &= \frac{m}{4\pi r^3+\alpha m}[3(1-\frac{\alpha}{r^2})+\alpha e^{-Ar^2}(11B^2r^2-\frac{9}{2}ABr^2+\frac{39}{4r^2}-\frac{1}{4}A-\frac{11}{4} \\
&\times B+\frac{\beta}{2}(A+B-\frac{2}{r^2}))], \qquad (11)\\
p_r^{eff} &= \frac{m}{4\pi r^3+\alpha m}[1-\frac{\alpha}{r^2}+\alpha e^{-Ar^2}(3A^2r^2+2B^2r^2-\frac{5}{2}ABr^2-\frac{15}{4}A-\frac{1}{4}B \\
&+ \frac{13}{4r^2}-\frac{\beta}{2}(A+B+\frac{4}{r^2}))], \qquad (12)\\
p_t^{eff} &= \frac{m}{4\pi r^3+\alpha m}[(1+\beta)(1-\frac{\alpha}{r^2})+\alpha e^{-Ar^2}(2B^2r^2-\frac{5}{2}ABr^2-\frac{1}{4}A+\frac{11}{4}B \\
&+ \frac{45}{4r^2}+\beta(B^2r^2-ABr^2+A+3B+\frac{8}{r^2}))]. \qquad (13)
\end{aligned}$$

For $\mathcal{L}_m = -p_t$, the field equations take the form

$$\begin{aligned}
\rho^{eff} &= \frac{m}{4\pi r^3+(1+\beta)\alpha m}[3(1-\frac{\alpha}{r^2})+\alpha e^{-Ar^2}(11B^2r^2-\frac{9}{2}ABr^2+\frac{39}{4r^2}-\frac{1}{4} \\
&\times A-\frac{11}{4}B+\frac{\beta}{2}(A+B-\frac{2}{r^2}))], \qquad (14)\\
p_r^{eff} &= \frac{m}{4\pi r^3+(1+\beta)\alpha m}[1-\frac{\alpha}{r^2}+\alpha e^{-Ar^2}(3A^2r^2+2B^2r^2-\frac{5}{2}ABr^2-\frac{15}{4}A \\
&- \frac{1}{4}B+\frac{13}{4r^2}-\frac{\beta}{2}(A+B+\frac{4}{r^2}))], \qquad (15)\\
p_t^{eff} &= \frac{m}{4\pi r^3+(1+\beta)\alpha m}[(1+\beta)(1-\frac{\alpha}{r^2})+\alpha e^{-Ar^2}(2B^2r^2-\frac{5}{2}ABr^2-\frac{1}{4}A \\
&+ \frac{11}{4}B+\frac{45}{4r^2}+\beta(B^2r^2-ABr^2+A+3B+\frac{8}{r^2}))]. \qquad (16)
\end{aligned}$$

3 Physical Behavior

In this section, we discuss physical behavior and stability criteria of compact stars in the presence of anisotropic pressure. The Schwarzschild solution is known as the best choice to describe the exterior of compact stars given as [13]

$$ds_+^2 = (1-\frac{2M}{r})dt^2-(1-\frac{2M}{r})^{-1}dr^2-r^2(d\theta^2+r^2\sin^2\theta d\phi^2). \qquad (17)$$

At the surface of the star $r = R$, the smooth matching of the interior solution to the vacuum exterior solution yields

$$g_{tt}^{-} = g_{tt}^{+}, \quad g_{rr}^{-} = g_{rr}^{+}, \quad g_{tt,r}^{-} = g_{tt,r}^{+}, \tag{18}$$

where $-$ and $+$ describe interior and exterior solutions, respectively. The matching of these exterior and interior solutions leads to

$$A = -\frac{1}{R^2}\ln\left(1-\frac{2M}{R}\right), \tag{19}$$

$$B = \frac{M}{R^3}\left(1-\frac{2M}{R}\right)^{-1}, \tag{20}$$

$$C = \ln\left(1-\frac{2M}{R}\right) - \frac{M}{R}\left(1-\frac{2M}{R}\right)^{-1}. \tag{21}$$

For masses and radii of considered rapidly rotating neutron stars, the corresponding values of constants A and B are given in Table **1**.

Table 1: Approximate values of unknown parameters for the proposed compact stars.

Compact Stars	M	$R(km)$	$\frac{M}{R}$	$A(km^{-2})$	$B(km^{-2})$
Her X-1	$0.88M_{\odot}$	7.7	0.168	0.0069027643	0.00426736462
SAX J 1808.4-3658	$1.435M_{\odot}$	7.07	0.299	0.0182315697	0.01488011569
4U 1820-30	$2.25M_{\odot}$	10.0	0.332	0.0109064412	0.00988095238

3.1 Maximality Condition

The dense nature of compact stars demands that the influence of effective energy density, radial and transverse pressures should be positive, finite and maximum in the interior of compact stars. The graphical analysis of effective energy density, radial and transverse pressures for both choices of $\mathcal{L}_m$ is shown in Figures **1-3**. These figures indicate that ρ^{eff}, p_r^{eff} and p_t^{eff} have larger values near the center of each star and start decreasing near the surface of the stars. In order to investigate maximum behavior of effective energy density and radial pressure at $r = 0$, the maximality conditions yield

$$\frac{d\rho^{eff}}{dr} = 0, \quad \frac{dp_r^{eff}}{dr} = 0, \quad \frac{d^2\rho^{eff}}{dr^2} < 0, \quad \frac{d^2p_r^{eff}}{dr^2} < 0.$$

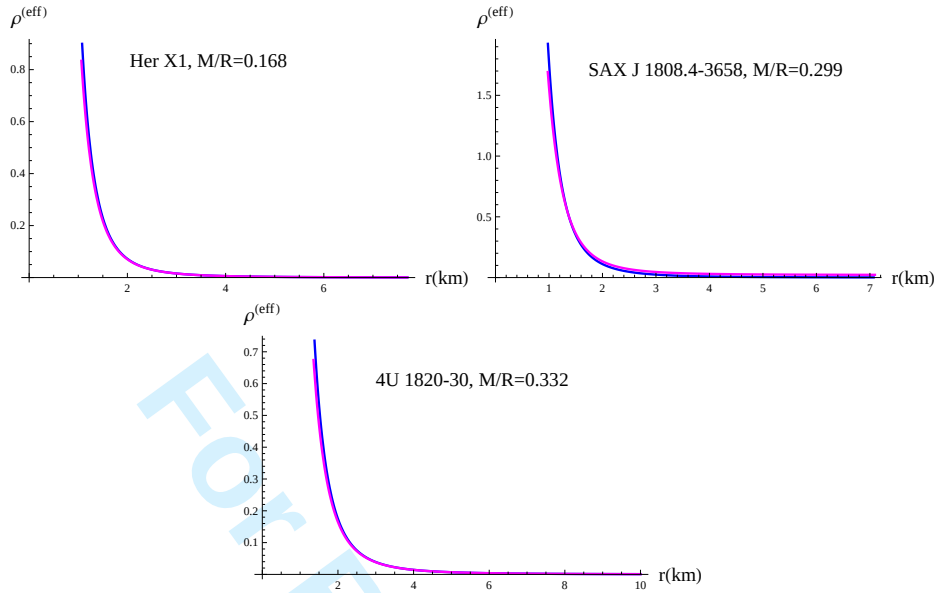

Figure 1: Behavior of $\rho^{eff}(kgm^{-3})$ versus $r(km)$ for $\mathcal{L}_m = -p_r$ (blue) and $\mathcal{L}_m = -p_t$ (magenta), $\alpha = 2$, $\beta = 1$.

To verify maximality conditions, we formulate the radial derivatives of Eqs.(11)-(13) as

$$\begin{aligned}
\frac{d\rho^{eff}}{dr} &= \frac{me^{-Ar^2}}{2r^3(4\pi r^3+\alpha m)^2}[12e^{Ar^2}(\alpha^2 m+10\alpha\pi r^3-6\pi r^5)+\alpha\{2\pi r^3(-44B^2 \\
&\times\ r^4+3Br^2(11-2\beta)+2A^2r^4(1+18Br^2-2\beta)+Ar^2(-75-88B^2r^4 \\
&-\ 4Br^2(\beta-10)+2\beta)+5(4\beta-39))+\alpha m(-39+44B^2r^4+A^2r^4(1 \\
&+\ 18Br^2-2\beta)+4\beta-Ar^2(39+44B^2r^4-4\beta+Br^2(2\beta+7)))\}], \quad (22) \\
\frac{dp_r^{eff}}{dr} &= \frac{me^{-Ar^2}}{2r^3(4\pi r^3+\alpha m)^2}[4e^{Ar^2}(\alpha^2 m+10\alpha\pi r^3-6\pi r^5)+\alpha\{2\pi r^3(-65-8 \\
&\times\ B^2r^4-24A^3r^6+40\beta+2A^2r^4(9+10Br^2+2\beta)+Ar^2(19-16B^2r^4 \\
&+\ 22\beta+4Br^2(\beta+3))+3Br^2(1+2\beta)+\alpha m(-13+8B^2r^4-12A^3r^6 \\
&+\ 8\beta+A^2r^4(27+10Br^2+2\beta)+Ar^2(-13-8B^2r^4+8\beta+Br^2(2\beta \\
&-\ 9)))\}], \quad (23)
\end{aligned}$$

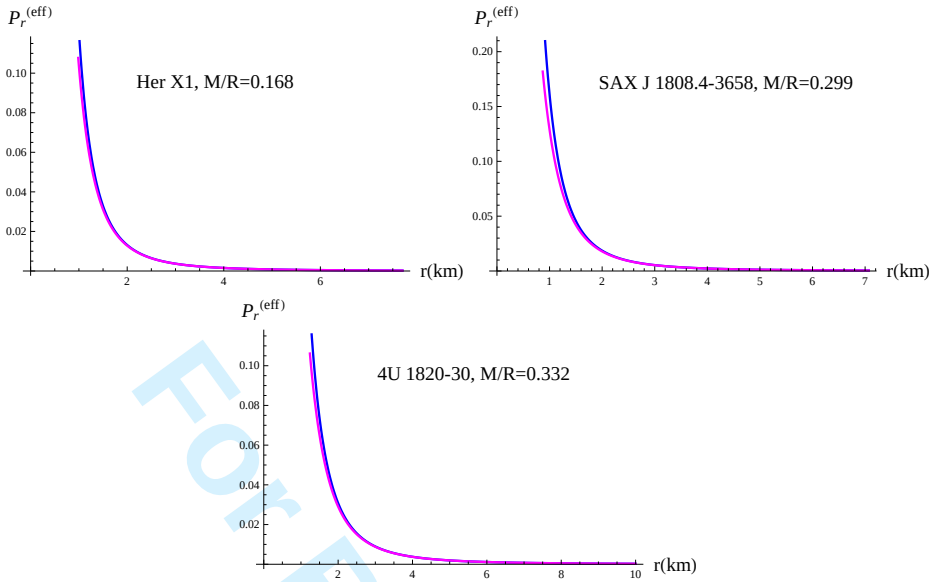

Figure 2: Plot of $p_r^{eff}(kgm^{-1}s^{-2})$ versus $r(km)$ for $\mathcal{L}_m = -p_r$ (blue) and $\mathcal{L}_m = -p_t$ (magenta), $\alpha = 2$, $\beta = 1$.

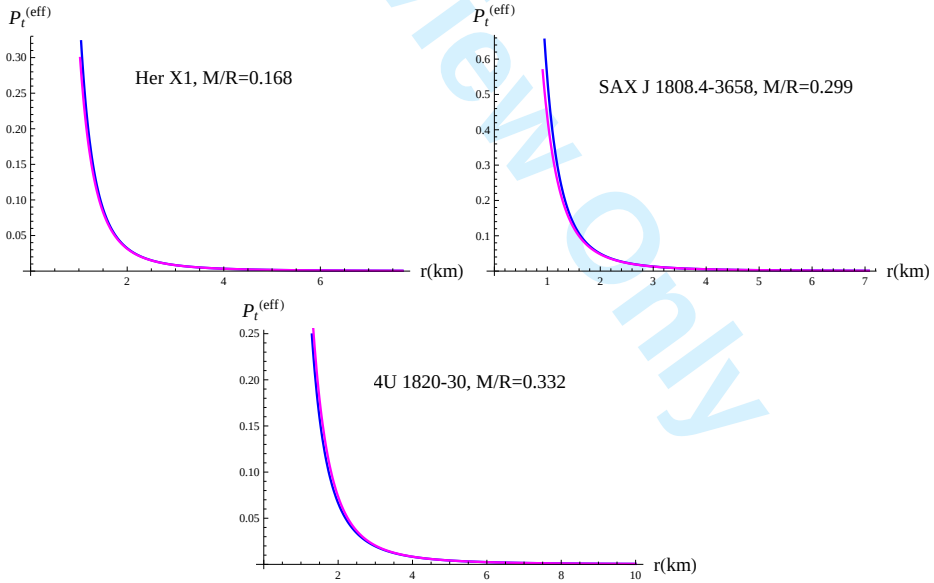

Figure 3: Evolution of $p_t^{eff}(kgm^{-1}s^{-2})$ versus $r(km)$ for $\mathcal{L}_m = -p_r$ (blue) and $\mathcal{L}_m = -p_t$ (magenta), $\alpha = 2$, $\beta = 1$.

$$\frac{dp_t^{eff}}{dr} = \frac{me^{-Ar^2}}{2r^3(4\pi r^3+\alpha m)^2}[-4e^{Ar^2}(6\pi r^5-\alpha^2 m-10\alpha\pi r^3)(1+\beta)+\alpha\{-2\pi r^3 \times (225+3Br^2(11-2\beta)-4B^2r^4(\beta-2)-160\beta+2A^2r^4(-1-4\beta+2 \times Br^2(2\beta-5))+Ar^2(87-8B^2r^4(\beta-2)-76\beta-4Br^2(5\beta-3))+\alpha \times m(-45-4B^2r^4(\beta-2)+32\beta+A^2r^4(1+2Br^2(5-2\beta)+4\beta)+Ar^2 \times (-45+4B^2r^4(\beta-2)+32\beta+Br^2(16\beta-21)))\}], \quad (24)$$

The radial derivatives of Eqs.(14)-(16) are given by

$$\frac{d\rho^{eff}}{dr} = \frac{me^{-Ar^2}}{2r^3(4\pi r^3+\alpha m(1+\beta))^2}[12e^{Ar^2}(\alpha^2 m(1+\beta)+10\alpha\pi r^3-6\pi r^5)+\alpha\{2 \times \pi r^3(-44B^2r^4+3Br^2(11-2\beta)+2A^2r^4(1+18Br^2-2\beta)+Ar^2(-75 - 88B^2r^4-4Br^2(\beta-10)+2\beta)+5(4\beta-39))+\alpha m(1+\beta)(-39+44 \times B^2r^4+A^2r^4(1+18Br^2-2\beta)+4\beta-Ar^2(39+44B^2r^4-4\beta+Br^2(2 \times \beta+7)))\}], \quad (25)$$

$$\frac{dp_r^{eff}}{dr} = \frac{me^{-Ar^2}}{2r^3(4\pi r^3+\alpha m(1+\beta))^2}[4e^{Ar^2}(\alpha^2 m(1+\beta)+10\alpha\pi r^3-6\pi r^5)+\alpha\{2 \times \pi r^3(-65-8B^2r^4-24A^3r^6+40\beta+3Br^2(1+2\beta)+2A^2r^4(9+10B \times r^2+2\beta)+Ar^2(19-16B^2r^4+22\beta+4Br^2(\beta+3))+\alpha m(1+\beta)(-13 + 8B^2r^4-12A^3r^6+8\beta+A^2r^4(27+10Br^2+2\beta)+Ar^2(-13+8\beta-8 \times B^2r^4+Br^2(2\beta-9)))\}], \quad (26)$$

$$\frac{dp_t^{eff}}{dr} = \frac{me^{-Ar^2}}{2r^3(4\pi r^3+\alpha m(1+\beta))^2}[\alpha\{(4\pi r^3+\alpha m(1+\beta))(-45+8B^2r^4-32\beta + 4B^2r^4\beta+4e^{Ar^2}(1+\beta)+A^2r^4(1-4\beta+2Br^2(2\beta+5))-Ar^2(45+32 \times \beta+4B^2r^4(\beta+2)+Br^2(16\beta+21)))-6\pi(4e^{Ar^2}(1+\beta)(r^2-\alpha)+\alpha \times (45+32\beta+4B^2r^4(\beta+2)+Br^2(12\beta+11)-Ar^2(1-4\beta+2Br^2(5 + 2\beta)))\}]. \quad (27)$$

For $\mathcal{L}_m = -p_r$, the second radial derivatives of effective energy density, radial and transverse pressures become

$$\frac{d^2\rho^{eff}}{dr^2} = \frac{me^{-Ar^2}}{2r^4(4\pi r^3+\alpha m)^3}[36e^{Ar^2}(-\alpha^3m^2-4\alpha m\pi r^3(3\alpha+r^2)+16\pi^2(2r^8-5 \times \alpha r^6))+\alpha\{-16\pi^2r^6(-585-44B^2r^4+6Br^2(11-2\beta)+2A^3r^6(1+18$$

$$
\begin{aligned}
&\times\ Br^2-2\beta)+60\beta-A^2r^4(73+88B^2r^4+4Br^2(\beta-10)+2\beta)+Ar^2\\
&\times\ (-345-44B^2r^4+Br^2(73-10\beta)+24\beta))+\alpha^2m^2(117+44B^2r^4-2\\
&\times\ A^3r^6(1+18Br^2-2\beta)-12\beta+A^2r^4(79+88B^2r^4-10\beta+4Br^2(17\\
&+\ \beta))-Ar^2(220B^2r^4+Br^2(7+2\beta)+3(4\beta-39)))-4\alpha m\pi r^3(4A^3r^6(1\\
&+\ 18Br^2-2\beta)+308B^2r^4+3Br^2(2\beta-11)+9(4\beta-39)-4A^2r^4(44B^2\\
&\times\ r^4+38-2\beta+Br^2(7+2\beta))+Ar^2(-471+176B^2r^4-2Br^2(41+4\\
&\times\ \beta)+54\beta))\}], \qquad (28)
\end{aligned}
$$

$$
\begin{aligned}
\frac{d^2p_r^{eff}}{dr^2} &= \frac{-me^{-Ar^2}}{2r^4(4\pi r^3+\alpha m)^3}[12e^{Ar^2}(\alpha^3m^2+4\alpha m\pi r^3(3\alpha+r^2)+\pi^2(80\alpha r^6-32\\
&\times\ r^8))+\alpha\{-4\alpha m\pi r^3(117-56B^2r^4+48A^4r^8+Ar^2(201-32B^2r^4+2\\
&\times\ Br^2(33-4\beta)-90\beta)+4A^2r^4(-23+8B^2r^4+Br^2(9-2\beta)-10\beta)\\
&+\ 3Br^2(1+2\beta)-72\beta-4A^3r^6(27+10Br^2+2\beta))+\alpha^2m^2(-39-8B^2\\
&\times\ r^4-24A^4r^8+24\beta+2A^3r^6(45+10Br^2+2\beta)+A^2r^4(-53-16B^2r^4\\
&+\ 4Br^2(\beta-12)+14\beta)+Ar^2(-39+40B^2r^4+Br^2(9-2\beta)+24\beta))\\
&-\ 16\pi^2r^6(195+8B^2r^4+24A^4r^8-120\beta-6Br^2(1+2\beta)-2A^3r^6(9+10\\
&\times\ Br^2+2\beta)+A^2r^4(-37+16B^2r^4-26\beta-4Br^2(3+\beta))+Ar^2(27+8\\
&\times\ B^2r^4-84\beta-5Br^2(3+2\beta)))\}], \qquad (29)
\end{aligned}
$$

$$
\begin{aligned}
\frac{d^2p_t^{eff}}{dr^2} &= \frac{-me^{-Ar^2}}{2r^4(4\pi r^3+\alpha m)^3}[-12e^{Ar^2}(-\alpha^3m^2-4\alpha m\pi r^3(3\alpha+r^2)+16\pi^2(2r^8-5\\
&\times\ \alpha r^6))(1+\beta)+\alpha\{-16\pi^2r^6(675+Ar^2(399+Br^2(45-56\beta)-4B^2r^4(\beta\\
&-\ 2)-312\beta)+6Br^2(11-12\beta)-4B^2r^4(\beta-2)-480\beta+2A^3r^6(-1-4\\
&\times\ \beta+2Br^2(2\beta-5))+A^2r^4(85-8B^2r^4(\beta-2)-84\beta-4Br^2(5\beta-3)))\\
&+\ \alpha^2m^2(-135+4B^2r^4(\beta-2)+96\beta+2A^3r^6(1+2Br^2(5-2\beta)+4\beta)\\
&+\ Ar^2(-135+Br^2(21-16\beta)-20B^2r^4(\beta-2)+96\beta)+A^2r^4(-91+8\\
&\times\ B^2r^4(\beta-2)+60\beta+4Br^2(11\beta-18)))-4\alpha m\pi r^3(405+28B^2r^4(\beta-2)\\
&-\ 288\beta+3Br^2(12\beta-11)+4A^3r^6(-1-4\beta+2Br^2(2\beta-5))+Ar^2(543\\
&+\ 16B^2r^4(\beta-2)-372\beta-38Br^2(2\beta-3))-4A^2r^4(-44+4B^2r^4(\beta-2)\\
&+\ 36\beta+Br^2(16\beta-21)))\}]. \qquad (30)
\end{aligned}
$$

The second derivatives of effective energy density, radial and transverse pressures for $\mathcal{L}_m=-p_t$ turn out to be

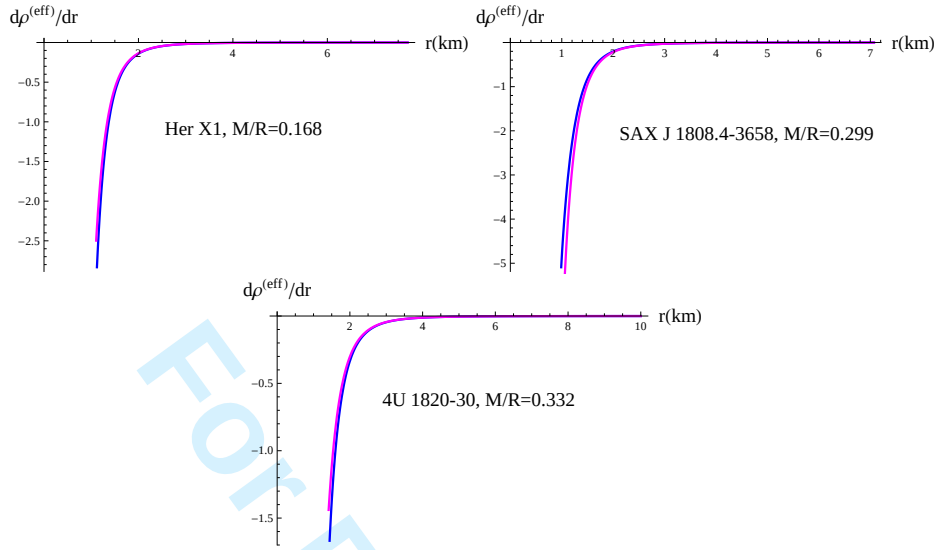

Figure 4: Plot of $\frac{d\rho^{eff}}{dr}$ versus r for $\mathcal{L}_m = -p_r$ (blue) and $\mathcal{L}_m = -p_t$ (magenta), $\alpha = 2$, $\beta = 1$.

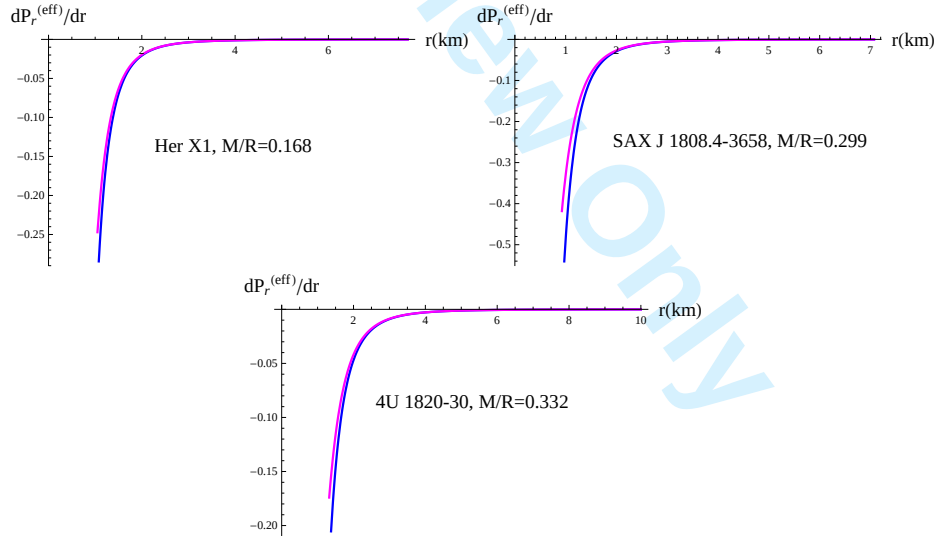

Figure 5: Plot of $\frac{dp_r^{eff}}{dr}$ versus r for $\mathcal{L}_m = -p_r$ (blue) and $\mathcal{L}_m = -p_t$ (magenta), $\alpha = 2$, $\beta = 1$.

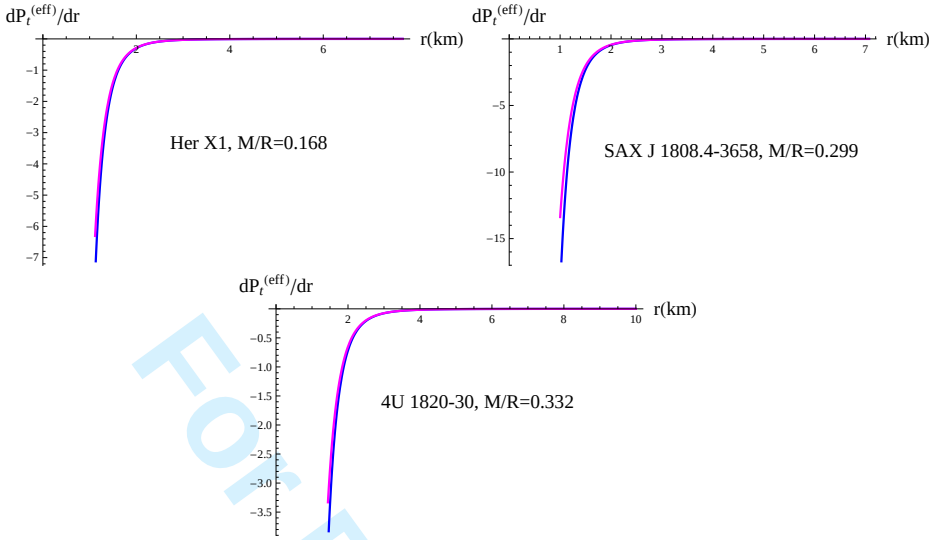

Figure 6: Variation of $\frac{dp_t^{eff}}{dr}$ versus r for $\mathcal{L}_m = -p_r$ (blue) and $\mathcal{L}_m = -p_t$ (magenta), $\alpha = 2$, $\beta = 1$.

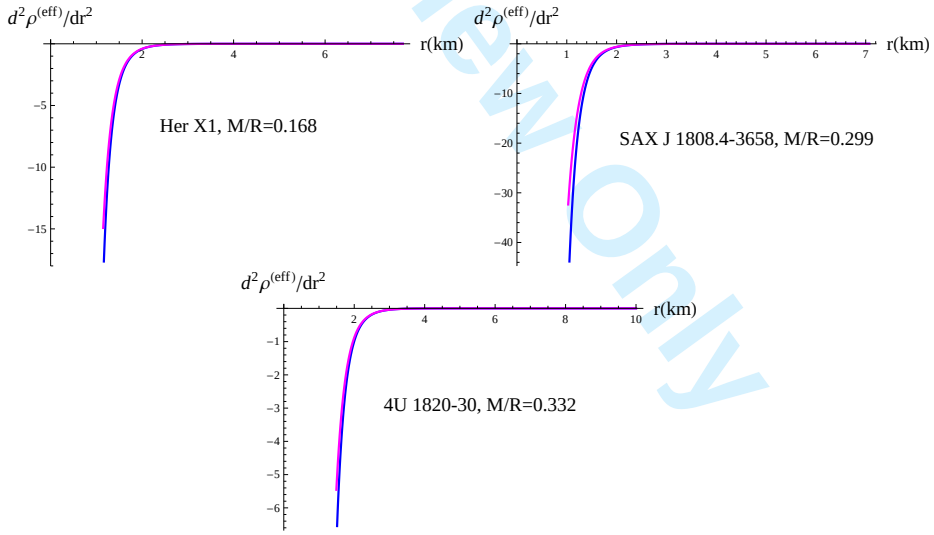

Figure 7: Variation of $\frac{d^2\rho^{eff}}{dr^2}$ versus r for $\mathcal{L}_m = -p_r$ (blue) and $\mathcal{L}_m = -p_t$ (magenta), $\alpha = 2$, $\beta = 1$.

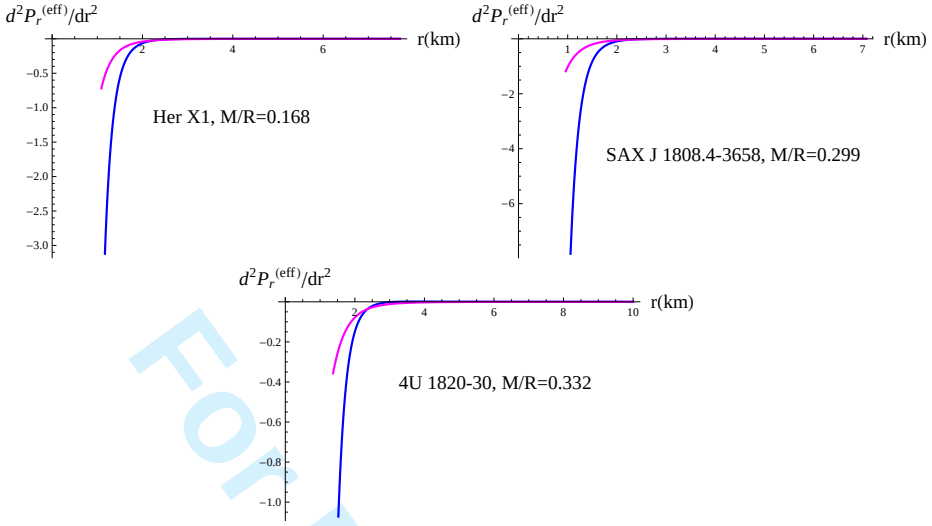

Figure 8: Variation of $\frac{d^2p_r^{eff}}{dr^2}$ versus r for $\mathcal{L}_m = -p_r$ (blue) and $\mathcal{L}_m = -p_t$ (magenta), $\alpha = 2$, $\beta = 1$.

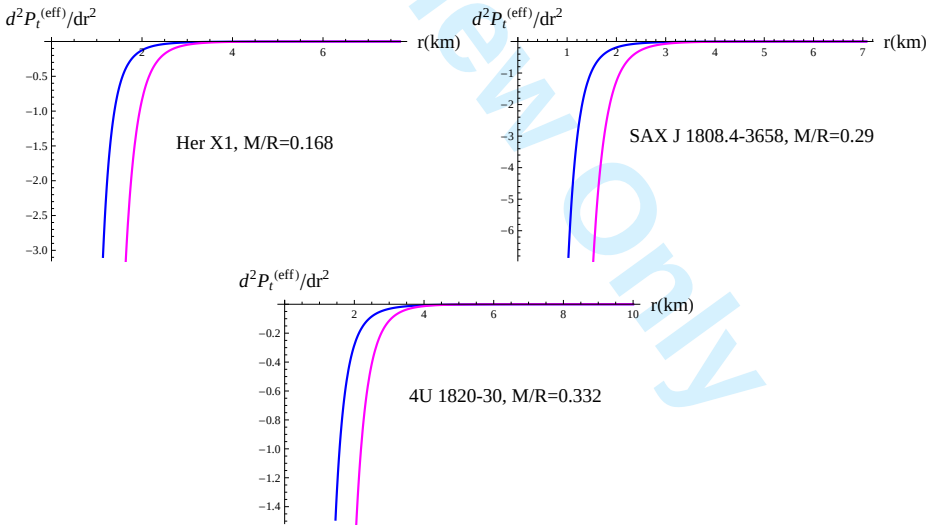

Figure 9: Variation of $\frac{d^2p_t^{eff}}{dr^2}$ versus r for $\mathcal{L}_m = -p_r$ (blue) and $\mathcal{L}_m = -p_t$ (magenta), $\alpha = 2$, $\beta = 1$.

$$\begin{aligned}
\frac{d^2\rho^{eff}}{dr^2} &= \frac{me^{-Ar^2}}{2r^4(4\pi r^3+\alpha m(1+\beta))^3}[36e^{Ar^2}(16\pi^2(2r^8-5\alpha r^6)-4\alpha m\pi r^3(3\alpha+r^2)\\
&\times (1+\beta)-\alpha^3m^2(1+\beta)^2)+\alpha\{-16\pi^2r^6(-585-44B^2r^4+6Br^2(11-2\\
&\times \beta)+2A^3r^6(1+18Br^2-2\beta)+60\beta-A^2r^4(73+88B^2r^4+4(\beta-10)B\\
&\times r^2+2\beta)+Ar^2(-345-44B^2r^4+Br^2(73-10\beta)+24\beta))+\alpha^2m^2(117\\
&+ 44B^2r^4-2A^3r^6(1+18Br^2-2\beta)-12\beta+A^2r^4(79+88B^2r^4+4Br^2\\
&\times (17+\beta)-10\beta)-Ar^2(220B^2r^4+Br^2(7+2\beta)+3(4\beta-39)))-4\alpha m\\
&\times \pi r^3(308B^2r^4+4A^3r^6(1+18Br^2-2\beta)+3Br^2(2\beta-11)+9(4\beta-39)\\
&- 4A^2r^4(38+44B^2r^4-2\beta+Br^2(7+2\beta))+Ar^2(-471+176B^2r^4+54\\
&\times \beta-2Br^2(41+4\beta)))\}], \qquad (31)\\
\frac{d^2p_r^{eff}}{dr^2} &= \frac{-me^{-Ar^2}}{2r^4(4\pi r^3+\alpha m(1+\beta))^3}[12e^{Ar^2}(\pi^2(80\alpha r^6-32r^8)+4\alpha m\pi r^3(3\alpha+r^2)\\
&\times (1+\beta)+\alpha^3m^2(1+\beta)^2)+\alpha\{\alpha^2m^2(1+\beta)^2(-39-8B^2r^4+24\beta-24\\
&\times A^4r^8+2A^3r^6(45+10Br^2+2\beta)+A^2r^4(-53-16B^2r^4+4Br^2(\beta-12)\\
&+ 14\beta)+Ar^2(-39+40B^2r^4+Br^2(9-2\beta)+24\beta))-16\pi^2r^6(195+24\\
&\times A^4r^8+8B^2r^4-120\beta-6Br^2(1+2\beta)-2A^3r^6(9+10Br^2+2\beta)+A^2\\
&\times r^4(-37+16B^2r^4-26\beta-4Br^2(3+\beta))+Ar^2(27+8B^2r^4-84\beta-5\\
&\times Br^2(3+2\beta)))+4\alpha m\pi r^3(1+\beta)(56B^2r^4-48A^4r^8+9(8\beta-13)-3B\\
&\times r^2(1+2\beta)+4A^3r^6(27+10Br^2+2\beta)+4A^2r^4(23-8B^2r^4+Br^2(-9\\
&+ 2\beta)+10\beta)+Ar^2(-201+32B^2r^4+90\beta+2Br^2(4\beta-33)))\}], \qquad (32)\\
\frac{d^2p_t^{eff}}{dr^2} &= \frac{-me^{-Ar^2}}{2r^4(4\pi r^3+\alpha m(1+\beta))^3}[12e^{Ar^2}(1+\beta)(\pi^2(80\alpha r^6-32r^8)+4\alpha m\pi r^3\\
&\times (3\alpha+r^2)(1+\beta)+\alpha^3m^2(1+\beta)^2)+\alpha\{4\alpha m\pi r^3(1+\beta)(3(11+12\beta)\\
&\times Br^2+28B^2r^4(\beta+2)-9(45+32\beta)+Ar^2(-543+16B^2r^4(\beta+2)\\
&- 38Br^2(2\beta+3)-372\beta)+4A^3r^6(1-4\beta+2Br^2(5+2\beta))-4A^2r^4\\
&\times (44+4B^2r^4(\beta+2)+36\beta+Br^2(16\beta+21)))+\alpha^2m^2(1+\beta)^2(-4B^2\\
&\times r^4(\beta+2)-3(32\beta+45)+2A^3r^6(1-4\beta+2Br^2(2\beta+5))-A^2r^4(91\\
&+ 8B^2r^4(\beta+2)+60\beta+4Br^2(11\beta+18))+Ar^2(20B^2r^4(\beta+2)+B\\
&\times r^2(16\beta+21)-3(45+32\beta)))+16\pi^2r^2(-4B^2r^4(2+\beta)-6Br^2(11\\
&+ 12\beta)-15(45+32\beta)+2A^3r^6(1-4\beta+2Br^2(5+2\beta))-A^2r^4(84\beta\\
&+ 85+8B^2r^4(\beta+2)+4Br^2(3+5\beta))-Ar^2(399+312\beta+4(2+\beta)
\end{aligned}$$

$$\times \quad B^2r^4 + Br^2(45 + 56\beta)))\}]. \tag{33}$$

The graphical behavior of first and second order radial derivatives of effective energy density, radial and transverse pressures for $\mathcal{L}_m = -p_r$ and $\mathcal{L}_m = -p_t$ is shown in Figures **4**-**9**. These graphs indicate that the first and second radial derivatives do not show any behavior exactly at $r = 0$. The first radial derivatives are non-zero and the second radial derivatives do not represent negative behavior at $r = 0$. We conclude that the effective energy density, radial and transverse pressures show maximum behavior near the center of stars but they do not satisfy the maximality conditions exactly at the center of compact stars.

3.2 Effective EoS Parameter

The equation of state parameter describes an interesting relationship between pressure and energy density. The EoS parameter provides different phases of the universe like when ω lies between 0 and 1, it corresponds to the radiation dominated era. For anisotropic fluid, we define the effective radial and transverse EoS parameters as $\omega_r^{eff} = \frac{p_r^{eff}}{\rho^{eff}}$ and $\omega_t^{eff} = \frac{p_t^{eff}}{\rho^{eff}}$. For both choices of $\mathcal{L}_m$, these parameters remain the same given as

$$\begin{aligned}
\omega_r^{eff} &= [1 - \frac{\alpha}{r^2} + \alpha e^{-Ar^2}(3A^2r^2 + 2B^2r^2 - \frac{5}{2}ABr^2 - \frac{15}{4}A - \frac{1}{4}B + \frac{13}{4r^2} - \frac{\beta}{2} \\
&\times \quad (A + B + \frac{4}{r^2})]/[3(1 - \frac{\alpha}{r^2}) + \alpha e^{-Ar^2}(11B^2r^2 - \frac{9}{2}ABr^2 + \frac{39}{4r^2} - \frac{1}{4}A \\
&- \quad \frac{11}{4}B + \frac{\beta}{2}(A + B - \frac{2}{r^2})], \qquad (34) \\
\omega_t^{eff} &= [(1 + \beta)(1 - \frac{\alpha}{r^2}) + \alpha e^{-Ar^2}(2B^2r^2 - \frac{5}{2}ABr^2 - \frac{1}{4}A + \frac{11}{4}B + \frac{45}{4r^2} + \beta \\
&\times \quad (B^2r^2 - ABr^2 + A + 3B + \frac{8}{r^2})]/[3(1 - \frac{\alpha}{r^2}) + \alpha e^{-Ar^2}(11B^2r^2 - \frac{9}{2}AB \\
&\times \quad r^2 + \frac{39}{4r^2} - \frac{1}{4}A - \frac{11}{4}B + \frac{\beta}{2}(A + B - \frac{2}{r^2})]. \qquad (35)
\end{aligned}$$

The graphical analysis in Figures **10** and **11** represents that effective radial and transverse EoS parameters correspond to ordinary matter distribution, i.e., $0 < \omega_r^{eff} < 1$ and $0 < \omega_t^{eff} < 1$ which describes the radiating nature of matter in the interior of compact stars.

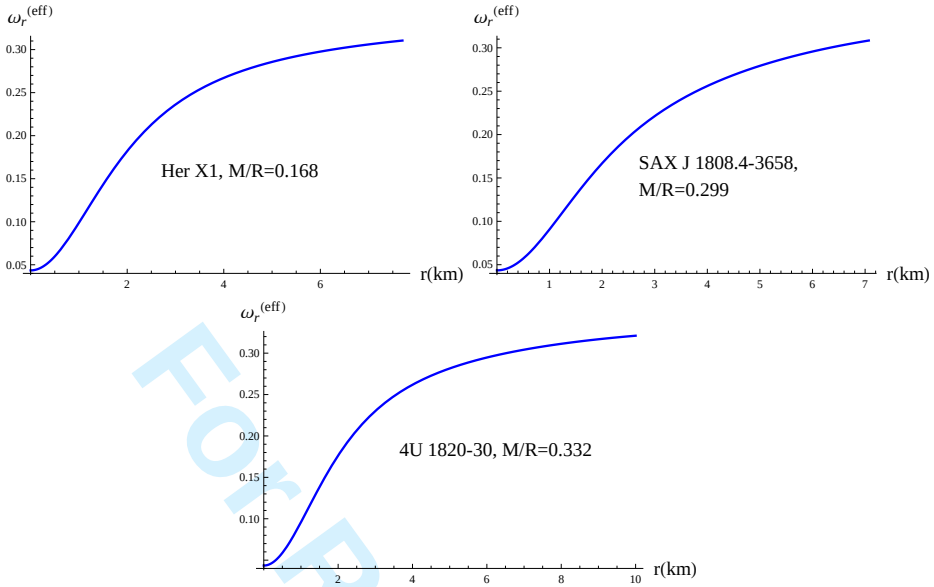

Figure 10: ω_r^{eff} versus r for $\alpha = 2$ and $\beta = 1$.

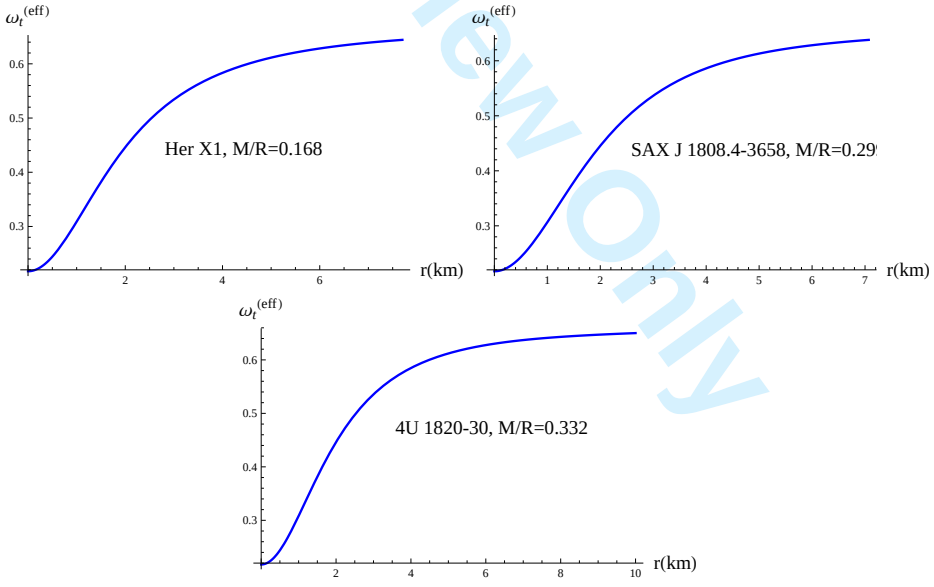

Figure 11: ω_t^{eff} versus r for $\alpha = 2$ and $\beta = 1$.

3.3 Anisotropic Factor

In the interior of compact stars, the effect of anisotropic pressure is analyzed by effective anisotropic factor $\Delta^{eff} = \frac{2}{r}(p_t^{eff} - p_r^{eff})$. For $\mathcal{L}_m = -p_r$, this factor takes the following form

$$\Delta^{eff} = \frac{me^{-Ar^2}}{r^3(4\pi r^3 + \alpha m)}[2r^2\beta e^{Ar^2} + \alpha\{16 - 6A^2r^2 + 24\beta + 2B^2r^4\beta + Br^2(5\beta + 6) - 2\beta e^{Ar^2} + Ar^2(7 + 3\beta - 2Br^2(2+\beta))\}], \quad (36)$$

whereas for $\mathcal{L}_m = -p_t$, this becomes

$$\Delta^{eff} = \frac{me^{-Ar^2}}{r^3(4\pi r^3 + \alpha m(1+\beta))}[2r^2\beta e^{Ar^2} + \alpha\{16 - 6A^2r^2 + 2B^2r^4\beta - 2\beta e^{Ar^2} + Br^2(5\beta + 6) + 24\beta + Ar^2(7 + 3\beta - 2Br^2(2+\beta))\}]. \quad (37)$$

If $p_t^{eff} > p_r^{eff}$, then $\Delta^{eff} > 0$ showing the outward direction of anisotropic pressure whereas for $p_t^{eff} < p_r^{eff}$, $\Delta^{eff} < 0$ which indicates the inward direction of anisotropic pressure. The graphical behavior of anisotropic measurement for considered compact star models is given in Figure **12**. For both choices of $\mathcal{L}_m$, the variation of anisotropy parameter is positive which yields a repulsive force that allows the formation of more massive distribution in the interior of compact stars.

3.4 Energy Conditions

The energy conditions play a dynamical role to investigate the exotic or ordinary nature of matter in the interior of compact stars. These conditions are classified as null energy condition (NEC), strong energy condition (SEC), dominant energy condition (DEC) and weak energy condition (WEC). For anisotropic fluid, the energy conditions are defined as

- NEC: $\rho^{eff} + p_r^{eff} \geq 0, \quad \rho^{eff} + p_t^{eff} \geq 0,$
- SEC: $\rho^{eff} + p_r^{eff} \geq 0, \quad \rho^{eff} + p_t^{eff} \geq 0, \quad \rho^{eff} + p_r^{eff} + 2p_t^{eff} \geq 0,$
- DEC: $\rho^{eff} \geq |p_r^{eff}|, \quad \rho^{eff} \geq |p_t^{eff}|,$
- WEC: $\rho^{eff} \geq 0, \quad \rho^{eff} + p_r^{eff} \geq 0, \quad \rho^{eff} + p_t^{eff} \geq 0.$

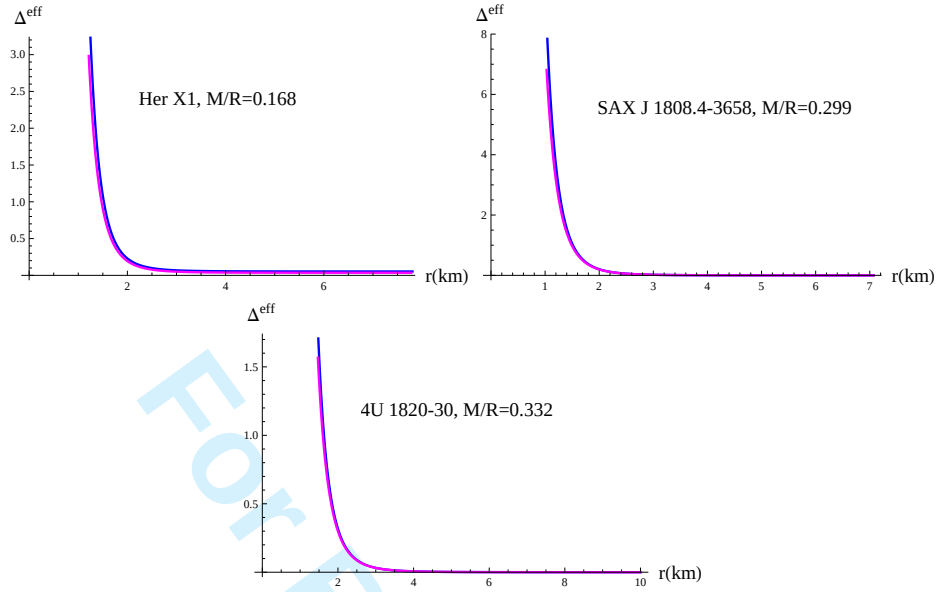

Figure 12: Δ^{eff} versus r for $\mathcal{L}_m = -p_r$ (blue) and $\mathcal{L}_m = -p_t$ (magenta), $\alpha = 2$, $\beta = 1$.

For all considered compact stars, the graphical analysis of these energy conditions remain the same, so we give the graphical behavior only for Her X-1 shown in Figure **13**. This shows that all conditions are satisfied which ensure the existence of ordinary matter in the interior of the proposed compact star models.

3.5 Stability Analysis

Here we analyze the stability criteria of compact star models through speed of sound to investigate the stable structure of compact stars. When the difference between transverse and radial components of speed of sound is positive, then the potentially stable regions are defined whereas for unstable regions, their difference does not satisfy the inequality $0 \leq \mid v_{st}^{2(eff)} - v_{sr}^{2(eff)} \mid \leq 1$ [24]. The potentially stable and unstable regions within the matter configuration are calculated from the difference of effective speed in radial and transverse directions. For anisotropic fluid with $\mathcal{L}_m = -p_r$, the effective radial $v_{sr}^{2(eff)}$ and transverse speeds $v_{st}^{2(eff)}$ yield

$$v_{sr}^{2(eff)} = [4e^{Ar^2}(\alpha^2 m + 10\alpha\pi r^3 - 6\pi r^5) + \alpha\{2\pi r^3(40\beta - 65 - 8B^2r^4 - 24A^3r^6$$

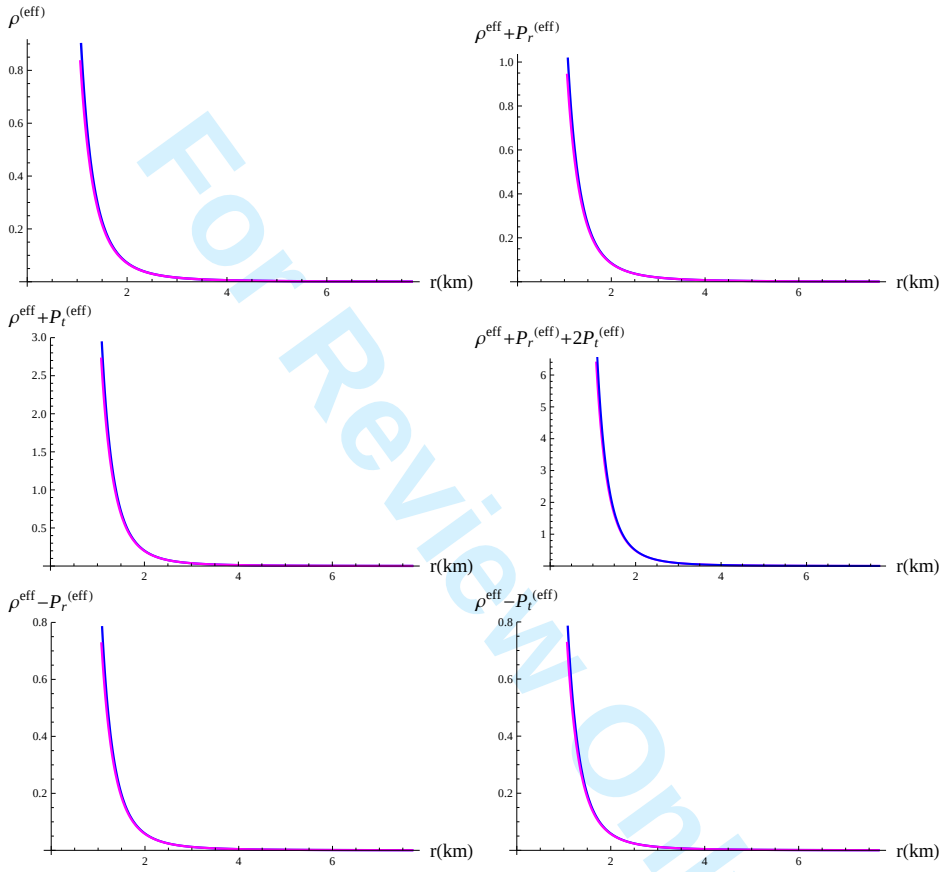

Figure 13: Energy conditions versus r corresponding to Her X-1 for $\mathcal{L}_m = -p_r$ (blue) and $\mathcal{L}_m = -p_t$ (magenta), $\alpha = 2$, $\beta = 1$.

$$
\begin{aligned}
&+ \; 3Br^2(1+2\beta)+2A^2r^4(9+10Br^2+2\beta)+Ar^2(19-16B^2r^4+4Br^2\\
&\times \; (\beta+3)+22\beta)+\alpha m(-13+8B^2r^4-12A^3r^6+8\beta+A^2r^4(27+10\\
&\times \; Br^2+2\beta)+Ar^2(-13-8B^2r^4+8\beta+Br^2(2\beta-9)))\}]/[12e^{Ar^2}(\alpha^2\\
&\times \; m+10\alpha\pi r^3-6\pi r^5)+\alpha\{2\pi r^3(-44B^2r^4+3Br^2(11-2\beta)+2A^2r^4\\
&\times \; (1+18Br^2-2\beta)+Ar^2(-75-88B^2r^4-4Br^2(\beta-10)+2\beta)+5\\
&\times \; (4\beta-39))+\alpha m(-39+44B^2r^4+A^2r^4(1+18Br^2-2\beta)+4\beta-Ar^2\\
&\times \; (39+44B^2r^4-4\beta+Br^2(2\beta+7)))\}], \qquad (38)
\end{aligned}
$$

$$
\begin{aligned}
v_{st}^{2(eff)} &= [-4e^{Ar^2}(6\pi r^5-\alpha^2 m-10\alpha\pi r^3)(1+\beta)+\alpha\{-2\pi r^3(225-4(\beta-2)B^2\\
&\times \; r^4+3Br^2(11-2\beta)-160\beta+2A^2r^4(-1-4\beta+2Br^2(2\beta-5))+Ar^2\\
&\times \; (87-8B^2r^4(\beta-2)-76\beta-4Br^2(5\beta-3))+\alpha m(-45-4(\beta-2)B^2\\
&\times \; r^4+32\beta+A^2r^4(1+2Br^2(5-2\beta)+4\beta)+Ar^2(-45+4B^2r^4(\beta-2)\\
&+ \; 32\beta+Br^2(16\beta-21)))\}]/[12e^{Ar^2}(\alpha^2 m+10\alpha\pi r^3-6\pi r^5)+\alpha\{2\pi r^3(3\\
&\times \; Br^2(11-2\beta)-44B^2r^4+2A^2r^4(1+18Br^2-2\beta)+Ar^2(-75-88B^2\\
&\times \; r^4-4Br^2(\beta-10)+2\beta)+5(4\beta-39))+\alpha m(-39+44B^2r^4+A^2r^4\\
&\times \; (1-2\beta+18Br^2)+4\beta-Ar^2(39+44B^2r^4-4\beta+Br^2(2\beta+7)))\}]. \qquad (39)
\end{aligned}
$$

For $\mathcal{L}_m=-p_t$, the effective radial and transverse speeds become

$$
\begin{aligned}
v_{sr}^{2(eff)} &= [4e^{Ar^2}(\alpha^2 m(1+\beta)+10\alpha\pi r^3-6\pi r^5)+\alpha\{2\pi r^3(-65-8B^2r^4-24A^3\\
&\times \; r^6+40\beta+3Br^2(1+2\beta)+2A^2r^4(9+10Br^2+2\beta)+Ar^2(19-16B^2\\
&\times \; r^4+22\beta+4Br^2(\beta+3))+\alpha m(1+\beta)(-13+8B^2r^4-12A^3r^6+A^2\\
&\times \; r^4(27+10Br^2+2\beta)+8\beta+Ar^2(-13+8\beta-8B^2r^4+(2\beta-9)B\\
&\times \; r^2))\}]/[12e^{Ar^2}(\alpha^2 m(1+\beta)+10\alpha\pi r^3-6\pi r^5)+\alpha\{2\pi r^3(-44B^2r^4+3\\
&\times \; Br^2(11-2\beta)+2A^2r^4(1+18Br^2-2\beta)+Ar^2(-75-88B^2r^4-4B\\
&\times \; r^2(\beta-10)+2\beta)+5(4\beta-39))+\alpha m(1+\beta)(-39+44B^2r^4+A^2r^4\\
&\times \; (1+18Br^2-2\beta)+4\beta-Ar^2(39+44B^2r^4-4\beta+Br^2(2\beta+7)))\}], \qquad (40)
\end{aligned}
$$

$$
\begin{aligned}
v_{st}^{2(eff)} &= [\alpha\{(4\pi r^3+\alpha m(1+\beta))(-45+8B^2r^4-32\beta+4B^2r^4\beta+4(1+\beta)\\
&\times \; e^{Ar^2}+A^2r^4(1-4\beta+2Br^2(2\beta+5))-Ar^2(45+32\beta+4(\beta+2)B^2\\
&\times \; r^4+Br^2(16\beta+21)))-6\pi(4e^{Ar^2}(1+\beta)(r^2-\alpha)+\alpha(45+32\beta+4\\
&\times \; B^2r^4(\beta+2)+Br^2(12\beta+11)-Ar^2(1-4\beta+2Br^2(5+2\beta)))\}]/[12
\end{aligned}
$$

$$\begin{aligned}
&\times\ e^{Ar^2}(\alpha^2 m(1+\beta)+10\alpha\pi r^3-6\pi r^5)+\alpha\{2\pi r^3(-44B^2r^4+3Br^2(11\\
&-\ 2\beta)+2A^2r^4(1+18Br^2-2\beta)+Ar^2(-75-88B^2r^4-4Br^2(\beta-10)\\
&+\ 2\beta)+5(4\beta-39))+\alpha m(1+\beta)(-39+A^2r^4(1+18Br^2-2\beta)+44\\
&\times\ B^2r^4+4\beta-Ar^2(39+44B^2r^4-4\beta+Br^2(2\beta+7)))\}]. \qquad (41)
\end{aligned}$$

For stable structure of compact stars, the speed of sound should be less than the speed of light. In Figures **14** and **15**, it is found that $0 \leq v_{sr}^{2(eff)} \leq 1$ and $0 \leq v_{st}^{2(eff)} \leq 1$ which describes the stable structure of the proposed compact stars. To analyze the potentially stable and unstable regions within the matter distribution, the difference of effective radial and transverse speeds for $\mathcal{L}_m = -p_r$ is calculated as

$$\begin{aligned}
v_{st}^{2(eff)}-v_{sr}^{2(eff)} &= 2[\alpha^2 m\{6A^3r^6+A^2r^4(\beta-13-2Br^2\beta)+2(-8+(6-B^2\\
&\times\ r^4+e^{Ar^2})\beta)+Ar^2(2B^2r^4\beta+4(3\beta-4)+Br^2(7\beta-6))\\
&+\ 2\pi r^3(-6r^2\beta e^{Ar^2}+\alpha(12A^3r^6+2B^2r^4\beta+3Br^2(5\beta-6)\\
&+\ 10(-8+(6+e^{Ar^2})\beta)+2A^2r^4(\beta-4-2Br^2\beta)+Ar^2(-53\\
&+\ 27\beta+4B^2r^4\beta+4Br^2(2\beta-3))))\}]/[12e^{Ar^2}(\alpha^2 m+10\alpha\pi r^3\\
&-\ 6\pi r^5)+\alpha\{2\pi r^3(-44B^2r^4+3Br^2(11-2\beta)+2A^2r^4(1+18\\
&\times\ Br^2-2\beta)+Ar^2(-75-88B^2r^4-4Br^2(\beta-10)+2\beta)+5\\
&\times\ (4\beta-39))+\alpha m(-39+44B^2r^4+4\beta+A^2r^4(1-2\beta+18\\
&\times\ Br^2)-Ar^2(Br^2(2\beta+7)+39+44B^2r^4-4\beta))\}]. \qquad (42)
\end{aligned}$$

When $\mathcal{L}_m = -p_t$, the difference of effective radial and transverse speed give

$$\begin{aligned}
v_{st}^{2(eff)}-v_{sr}^{2(eff)} &= -2[-\alpha^2 m(1+\beta)\{6A^3r^6+A^2r^4(-3\beta-13+2Br^2\beta)+2\\
&\times\ (-8+(-10+B^2r^4+e^{Ar^2})\beta)-Ar^2(2B^2r^4\beta+4(5\beta+4)\\
&+\ 3Br^2(3\beta+2))+2\pi r^3(6r^2\beta e^{Ar^2}+\alpha(80-12A^3r^6+100\beta\\
&+\ 2B^2r^4\beta+3Br^2(7\beta+6)-10e^{Ar^2}\beta+2A^2r^4(4+\beta(3-2B\\
&\times\ r^2))+Ar^2(53+49\beta+4B^2r^4\beta+12Br^2(\beta+1))))\}]/[12e^{Ar^2}\\
&\times\ (\alpha^2 m+10\alpha\pi r^3-6\pi r^5)+\alpha\{2\pi r^3(-44B^2r^4+3Br^2(11-2\\
&\times\ \beta)+2A^2r^4(1+18Br^2-2\beta)+Ar^2(-75-88B^2r^4-4Br^2\\
&\times\ (\beta-10)+2\beta)+5(4\beta-39))+\alpha m(-39+44B^2r^4+A^2r^4\\
&\times\ (1+18Br^2-2\beta)+4\beta-Ar^2(Br^2(2\beta+7)+39+44B^2r^4
\end{aligned}$$

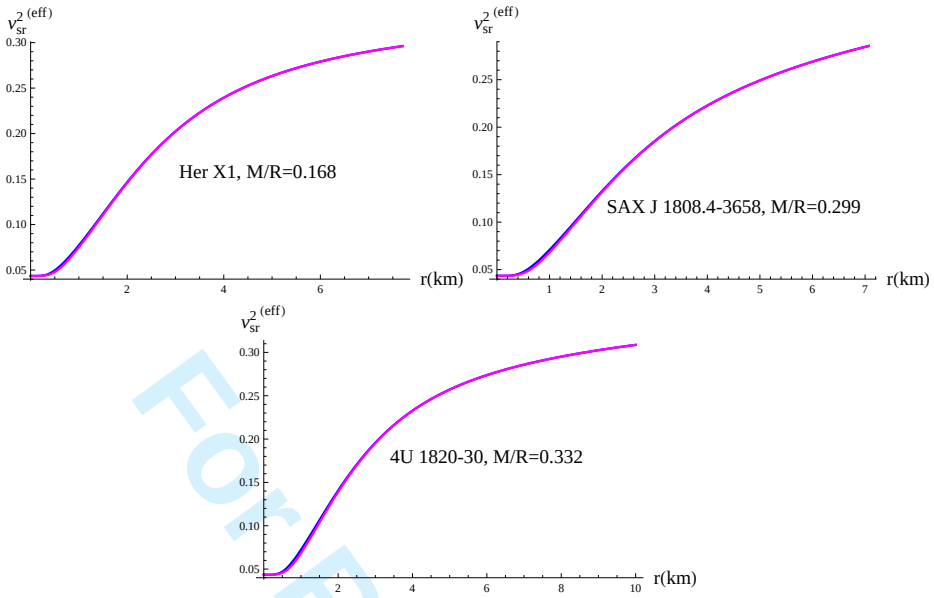

Figure 14: Radial speed versus r for $\mathcal{L}_m = -p_r$ (blue) and $\mathcal{L}_m = -p_t$ (magenta), $\alpha = 2$, $\beta = 1$.

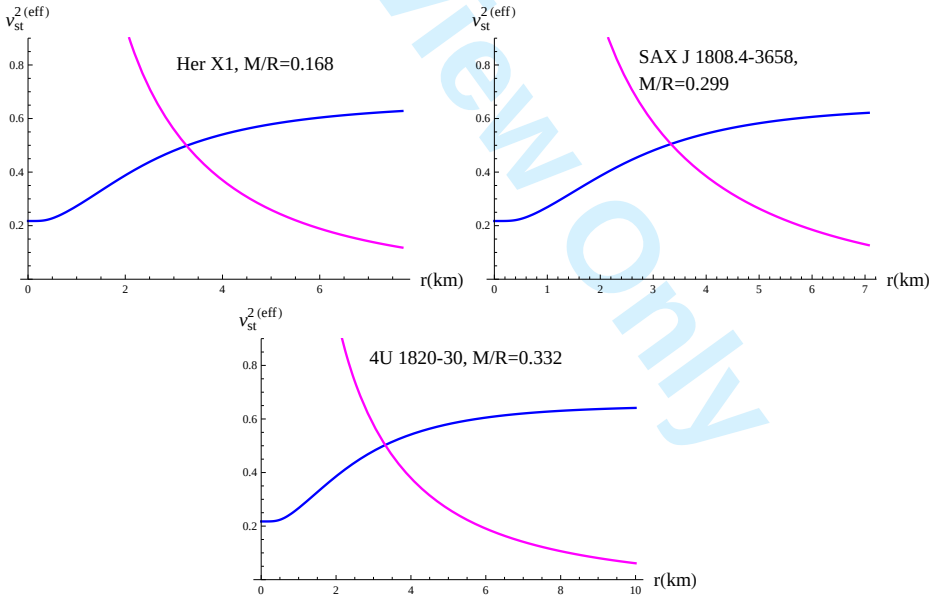

Figure 15: Transverse speed versus r for $\mathcal{L}_m = -p_r$ (blue) and $\mathcal{L}_m = -p_t$ (magenta), $\alpha = 2$, $\beta = 1$.

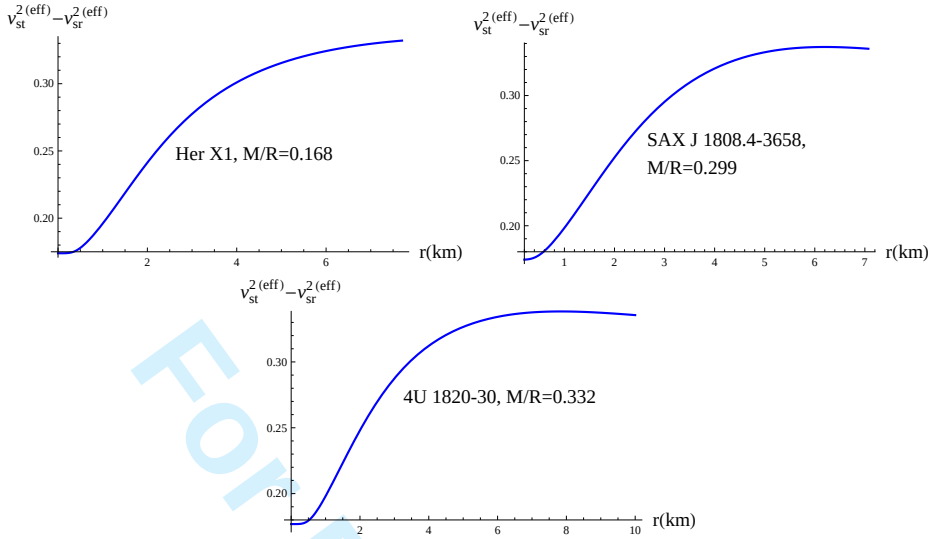

Figure 16: Behavior of $v_{st}^{2(eff)} - v_{sr}^{2(eff)}$ versus r for $\mathcal{L}_m = -p_r$ (blue), $\alpha = 2$, $\beta = 1$.

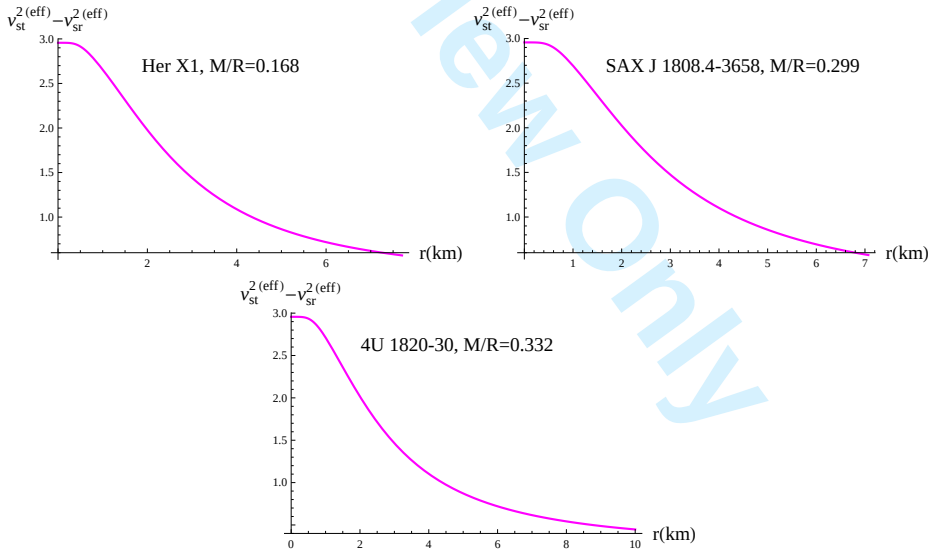

Figure 17: Behavior of $v_{st}^{2(eff)} - v_{sr}^{2(eff)}$ versus r for $\mathcal{L}_m = -p_t$ (magenta), $\alpha = 2$, $\beta = 1$.

$$- \quad 4\beta))\}]. \tag{43}$$

In Figure **16**, the behavior of $v_{st}^{2(eff)} - v_{sr}^{2(eff)}$ satisfies the inequality $0 \leq| v_{st}^{2(eff)} - v_{sr}^{2(eff)} |\leq 1$ for $\mathcal{L}_m = -p_r$ but in case of $\mathcal{L}_m = -p_t$, the inequality $0 \leq| v_{st}^{2(eff)} - v_{sr}^{2(eff)} |\leq 1$ does not hold as shown in Figure **17**. Thus, our considered compact star models are potentially stable for $\mathcal{L}_m = -p_r$ while $\mathcal{L}_m = -p_t$ leads to potentially unstable regions of stars.

4 Concluding Remarks

In this paper, we have studied physical features and stability of anisotropic compact stars in $f(R, T, R_{\mu\nu}T^{\mu\nu})$ gravity for a particular model $R+\alpha R_{\mu\nu}T^{\mu\nu}$. We have considered static spherically symmetric spacetime and applied the Krori-Barua metric solutions. The unknown constants A, B and C are determined through matching of interior and Schwarzschild exterior solutions. For masses and radii of proposed compact star models, the values of A, B and C are given in Table **1**. We have used the maximality conditions to describe the maximum behavior of effective energy density, radial and transverse pressures at the center of compact stars. We have also discussed the effective EoS parameter, anisotropic factor and energy conditions. We have analyzed the stability, potentially stable and unstable regions of compact stars via speed of sound. The graphical analysis corresponding to two different choices of matter Lagrangian, i.e., $\mathcal{L}_m = -p_r$ and $\mathcal{L}_m = -p_t$ is given. We summarize our results as follows.

- The effective energy density, radial and transverse pressures do not possess maximum behavior exactly at the center of stars which describes the violation of maximality conditions of compact stars in this gravity model.

- The values of effective radial and transverse EoS parameters lie between 0 and 1 which represent the radiating nature in the interior of compact stars.

- The effective anisotropic factor is found to be positive which implies that a repulsive anisotropic force exists and allows the formation of more massive distribution.

- All energy conditions are satisfied for proposed compact stars which ensure the existence of ordinary matter in the interior of compact stars.
- The stability conditions are satisfied, i.e., the effective radial and transverse speed of sounds are less than the speed of light. It is found that the inequality $0 \leq \mid v_{st}^{2(eff)} - v_{sr}^{2(eff)} \mid \leq 1$ holds for $\mathcal{L}_m = -p_r$ which describes the potentially stable regions of compact stars but for $\mathcal{L}_m = -p_t$, this inequality is not satisfied.

It is worthwhile to mention here that all energy conditions, effective EoS parameter and stability condition are satisfied for $\alpha = 2$ and $\beta = 1$ only. Finally, we conclude that the considered compact stars with anisotropic internal configuration are potentially stable for $\mathcal{L}_m = -p_r$ but unstable for $\mathcal{L}_m = -p_t$ in this gravity.

References

[1] Baade, W. and Zwicky, F.: Phys. Rev. **46**(1934)76.

[2] Ruderman, R.: Ann. Rev. Astron. Astrophys. **10**(1972)427; Canuto, V. and Fassio-Canuto, L.: Phys. Rev. D **7**(1973)1601.

[3] Hossein, S.K.M. et al.: Int. J. Mod. Phys. D **21**(2012)1250088.

[4] Lobo, F.S.N.: Class. Quantum Grav. **23**(2006)2014.

[5] Hernandez, H. and Nunez, L.A.: Can. J. Phys. **82**(2004)29.

[6] Mak, M.K. and Harko, T.: Int. J. Mod. Phys. D **13**(2004)149.

[7] Paul, B.C. and Deb, R.: Astrophys. Space Sci. **354**(2014)421.

[8] Kalam, M., Rahaman, F., Molla, S. and Hossein, S.K.M.: Astrphys. Space Sci. **349**(2013)865.

[9] Perlmutter, S. et al.: Astrophys. J. **483**(1997)565; Riess, A.G. et al.: Astron. J. **116**(1998)1009; Spergel, D.N. et al.: Astrophys. J. Suppl. **148**(2003)175; Tegmark, M. et al.: Phys. Rev. D **69**(2004)03501.

[10] Nojiri, S. and Odinstov, S.D.: Phys. Rep. **505**(2011)59; Bamba, K. Capozziello, S. Nojiri, S. and Odinstov, S.D.: Astrophys. Space Sci. **342**(2012)155; Ferraro, R. and Fiorini, F.: Phys. Rev. D **75**(2007)084031; Nojiri, S., Odintsov, S.D.: Phys. Lett. B **631**(2005)1; Harko, T., Lobo, F.S.N., Nojiri, S. and Odinstov, S.D.: Phys. Rev. D **84**(2011)024020.

[11] Haghani, Z. et al.: Phys. Rev. D **88**(2013)044023.

[12] Mak, M.K. and Harko, T.: Proc. Roy. Soc. Lond. A **459**(2003)393; Eur. Phys. J. C **73**(2013)2585.

[13] Goswami, R., Nzioki, A.M., Maharaj, S.D. and Ghosh, S.G.: Phys. Rev. D **90**(2014)084011.

[14] Astashenok, A.V., Capozziello, S. and Odinstov, S.D.: J. Cosmol. Astropart. Phys. **12**(2013)040; Abbas, G., Zubair, M. and Mustafa, G.: Astrophys. Space Sci. **358**(2015)26.

[15] Zubair, M., Abbas, G. and Noureen, I.: Astrophys. Space Sci. **361**(2016)8.

[16] Abbas, G. et al.: Astrophys. Space Sci. **357**(2015)2.

[17] Abbas, G., Qaisar, S. and Jawad, A.: Astrophys. Space Sci. **359**(2015)57; Zubair, M. and Abbas, G.: Astrophys. Space Sci. **361**(2016)27.

[18] Odinstov, S.D. and Sáez-Gómes, D.: Phys. Lett. B **725**(2013)437.

[19] Sharif, M. and Zubair, M.: J. Phys. Soc. Jpn. **81**(2012)114005.

[20] Sharif, M. and Zubair, M.: J. Cosmol. Astropart. Phys. **12**(2013)079.

[21] Krori, K.D. and Barua, J.: J. Phys. A: Math. Gen. **8**(1975)508.

[22] Rahaman, F. et al.: Eur. Phys. J. C **72**(2012)2071.

[23] Heintzmann, H. and Hillebrandt, W.: Astron. Astrophys. **38**(1975)51.

[24] Herrera, L.: Phys. Lett. A **165**(1992)206.